Shock-induced temperatures of $CaMgSi_2O_6$†

Bob Svendsen and Thomas J. Ahrens

Seismological Laboratory,
California Institute of Technology,
Pasadena, CA, 91125.

Abstract

Optical radiation from shock-compressed crystal $CaMgSi_2O_6$ (diopside) constrains crystal $CaMgSi_2O_6$ Hugoniot temperatures of 3500-4800 K in the 150-170 GPa pressure range, while glass $CaMgSi_2O_6$, having a density 87% that of crystal $CaMgSi_2O_6$, achieves Hugoniot temperatures of 3600-3800 K in the 105-107 GPa pressure range. The radiation history of each of these materials implies that the shock-compressed states of each are highly absorptive, with effective absorption coefficients of $\gtrsim$500–1000 m^{-1}. Calculated Hugoniot states for these materials, when compared to the experimental results, imply that crystal $CaMgSi_2O_6$ Hugoniot states in the 150-170 GPa range represent a high-pressure phase (HPP) solid (or possibly liquid) phase with an STP density of $\approx$4100$\pm$200 kg/m^3, STP Grüneisen's parameter of $\approx$1.5$\pm$0.5 and STP HPP-LPP specific internal energy difference, $\Delta e_i^{\alpha-\beta}$, of 0.9$\pm$0.5 MJ/kg. These results are consistent with a $CaSiO_3$-$MgSiO_3$ perovskite high-pressure phase assemblage. For glass $CaMgSi_2O_6$, we have the same range of HPP properties, except that $\Delta e_i^{\alpha-\beta}$ is 2.3$\pm$0.5 MJ/kg, a strong indication that the glass $CaMgSi_2O_6$ Hugoniot states occupy the liquid-phase in the system $CaMgSi_2O_3$. Comparison of the pressure-temperature Hugoniot of crystal $CaMgSi_2O_6$ with the Hugoniots of its constituent oxides (*i.e.*, SiO_2, CaO and MgO) demonstrates the primary influence of the HPP STP density of these materials on the magnitude of the temperature in their shock-compressed states. The crystal $CaMgSi_2O_6$ pressure-temperature Hugoniot constrained by the experimental results lies at 2500-3000 K between 110 and 135 GPa, within the plausible range of lowermost-mantle temperature profiles.

† submitted to the Journal of Geophysical Research.

Introduction

Mg-Fe oxides and/or silicates are currently believed to dominate the composition of the Earth's mantle. $CaMgSi_2O_6$, which in mineral form is known as diopside, represents one of several pyroxene compositions relevant to investigations of composition of the Earth's mantle, and is the only natural pyroxene to form large, transparent single crystals suitable for shock-temperature investigation. The possibility that the Earth accreted inhomogeneously (*e.g.*, Turekian and Clark, 1969), or strongly differentiated during core formation (*e.g.*, Stevenson, 1981), implies that certain regions of the mantle, such as D'', may be composed of oxides and/or silicates of much more refractory elements, such as Ca and/or Al. A number of previous static and dynamic experimental efforts (*e.g.*, Liu, 1978, 1979a; Svendsen and Ahrens, 1983; Boslough *et al.*, 1984; Boslough *et al.*, 1986) and modeling efforts (*e.g.*, Ruff and Anderson, 1980) have directly or indirectly addressed this issue. In particular, calculations indicate that $CaMgSi_2O_6$ (Di) could be one of the earliest phases to condense out of the solar nebula (Grossman and Larimer, 1974), and so may be a major participant in inhomogeneous accretion. In this paper, we use the shock-induced radiation from Di to constrain its Hugoniot temperature. Combining these constraints with previous work on the mechanical response of Di to shock compression, we place constraints on the pressure-density-temperature equation-of-state of the high-pressure phase(s) (HPP's) of Di. The high-pressure ($\gtrsim$ 50-80 GPa: Svendsen and Ahrens, 1983) shock-compressed states of crystal Di are likely to represent an assemblage of $CaSiO_3$-$MgSiO_3$ perovskites (Liu, 1979b).

Experimental

We conducted the experiments on a two-stage, light-gas gun (*e.g.*, Jeanloz and Ahrens, 1980a; Figure 1). In these, a lexan-encased tantalum (Ta) flyer-plate, accelerated to velocities between 4.7 and 6.1 km/sec (Table IV), impacted a 1.5 mm-thick Ta and 6.1 km/sec (Table IV), impacted a 1.5 mm-thick Ta driver-plate in contact with an approximately 2 mm-thick (100)-oriented,

transparent crystal Di samples or 4 mm-thick, transparent glass Di samples (Table IV). We covered the free-surface of an aluminum mask to avoid observing radiation from the target's edge. Radiation from the target reflects from a mirror, propagates though an objective lens, and is directed by a (dichroic) pellicle beam splitter and two half-silvered beam splitters into 4 detectors filtered at nominal wavelengths of 450, 600, 750 and 900 nm. We recorded the signal from each detector with a Tektronix 485 single-sweep oscilloscope and a LeCroy (model 8081) 100-MHz transient recorder.

The densities of crystal Di samples (Table IV) agree well with the ideal value of 3277 kg/m^3 (Robie *et al.*, 1978). This is consistent with the microprobe analyses of our sample materials, given in Table I. The glass Di samples are about 13.6% less dense than the crystal samples; this is consistent with the density of glass Di used, for example, in spectroscopic studies (Binsted *et al.*, 1985).

As in previous studies (*e.g.*, Lyzenga, 1980; Boslough *et al.* 1984), we vapor-deposited 500-1000 nm of silver (Ag) on the sample, and then placed the Ag "film" in contact with the Ta driver plate to minimize radiation from an otherwise rough driver plate-sample interface. We expected this Ag film to absorb any radiation from the Ta-Ag interface, heat up much less than a mechanical Ta-$CaMgSi_2O_6$ interface (Urtiew and Grover, 1974), and contain no trapped gas that could also contribute to interface radiation (Boslough, 1984).

Data Analysis

Our data set consists of six experiments: four on diopside ($CaMgSi_2O_6$, Di) single-crystals (140, 141, 169 and 170, Table IV), and two on $CaMgSi_2O_6$ (Di) glass (196 and 197, Table IV). We record the radiation intensity from the target as a function of time at the wavelengths stated above. In Figures 2 and 3, we display examples of this data at 750 nm. The data shown in Figure 2 from crystal Di (shot 141, Table IV), while that shown in Figure 3 is from glass diopside (shot 197, Table IV). These radiation histories are representative of those at all

other observed wavelengths and in all other experiments. With the known radiation intensity of a standard lamp (Boslough, 1984) at the observed wavelengths, we transform this raw data into experimental spectral radiation intensities (in the form of spectral radiance) as a function of time. The radiance data for all experiments is listed in Table II.

As stated above, the target consists of a Ta driver-plate, Ag film layer and sample layer. Radiation from the target is first observed when the shock wave compresses the Ag film at the Ag-sample interface (t_o, Figure 2 or 3). As shown most clearly in Figure 3, the radiation intensity in all experiments rises sharply to a peak value, and then as the shock wave propagates into the sample, the intensity decays almost as quickly to a time-independent magnitude reflecting that of the shocked sample. Since the Ag film is almost certainly much hotter than the sample over the time scale of the experiment (Boslough, 1984; Svendsen and Ahrens, 1987), the strong decay of the initial radiation intensity is most likely due to shock-induced opacity of the shocked sample (Boslough, 1985). With the possible exception of Al_2O_3 (Bass *et al.*, 1987), all initially transparent materials studied so far (*e.g.*, LiF: Kormer, 1968; $CaAl_2Si_2O_8$: Boslough *et al.*, 1986) lose some transparency during shock compression. In the present case, the thermal radiation from Ag at the Ag-sample interface is apparently strongly absorbed by the shocked sample such that observed radiation intensity is quickly dominated by the sample intensity (Boslough, 1985). Hence we observe a fast decay of the initial high intensity and a subsequent time-independent radiation intensity displayed in Figures 2 and 3. To demonstrate these considerations from a model viewpoint, we represent the observed radiation intensity, $I_{\lambda exp}(\lambda,t)$, in terms of a model intensity, $I_{\lambda mod}(\lambda,t)$, as a function of wavelength (λ), and time after the onset of radiation from the target, t, *i.e.*,

$$I_{\lambda mod}(\lambda,t) = \hat{\epsilon}_{\lambda I}(t) I_{\lambda pl}[\lambda,T_I(t)] + \hat{\epsilon}_{\lambda S}(t)\, I_{\lambda pl}(\lambda,T_s) \qquad [1]$$

In [1], T_s is the shock-compressed (Hugoniot) sample (S) temperature assumed homogeneous, uniform and constant, and $T_I(t)$ is the temperature of Ag at the

Ag-sample interface (I), which may be time-dependent (Grover and Urtiew, 1974). Further,

$$\hat{\varepsilon}_{\lambda I}(t) \equiv [1-r_{\lambda FS}]\ \tau_{\lambda US}(t)\ [1-r_{\lambda SF}]\ \tau_{\lambda S}(t)\ [1-r_{\lambda INT}] \quad [2]$$

$$\hat{\varepsilon}_{\lambda S}(t) \equiv [1-r_{\lambda FS}]\ \tau_{\lambda US}(t)\ [1-r_{\lambda SF}]\ [1+r_{\lambda INT}\ \tau_{\lambda S}(t)]\ [1-\tau_{\lambda S}(t)] \quad [3]$$

are the effective normal spectral emissivities of the Ag at the Ag-sample interface and shocked sample, respectively, while $r_{\lambda FS}$, $r_{\lambda SF}$ and $r_{\lambda INT}$ are the effective normal spectral reflectivities of the unshocked sample (US) free-surface, shock front and Ag-sample interface, respectively. Also,

$$\tau_{\lambda US}(t) \equiv \exp[-a^*_{\lambda US}\ (1-t/t_{exp})] \quad [4]$$

and

$$\tau_{\lambda S}(t) \equiv \exp[-a^*_{\lambda S}\ t/t_{exp}] \quad [5]$$

are the effective normal spectral transmissivities of unshocked sample and shocked sample layers, respectively. In [4] and [5], $a^*_{\lambda US}$ and $a^*_{\lambda S}$ are nondimensional forms of the effective normal spectral coefficients of absorption in the unshocked and shocked samples, respectively, given by

$$a^*_{\lambda S} \equiv a_{\lambda S}\ (U-v_s)t_{exp} \quad [6]$$

and

$$a^*_{\lambda US} \equiv a_{\lambda US}\ Ut_{exp} \quad [7]$$

Note that $t_{exp} \equiv d/U$ is the experimental time-scale, U is the shock wave velocity in the sample, d is the initial thickness of the sample layer in the target, and v_s is the shock-induced material velocity of the shocked sample. Lastly, we have

$$I_{\lambda pl}(\lambda,T) \equiv \frac{C_1}{\lambda^5\ [e^{C_2/\lambda T} - 1]}$$

(with $C_1 \equiv 1.19088\times10^{-16}W\cdot m^2$ and $C_2 \equiv 1.4388\times10^{-2}m\cdot K$) as the Planck function.

Assuming the shocked sample is strongly absorptive, we have $a^*_{\lambda S} \gtrsim 1$ or $a_{\lambda S} \gtrsim 1/(d-v_s t_{exp})$ from [6], and so $\tau_{\lambda S}(t) \sim 0$ from [5]. In this case, $\hat{\epsilon}_{\lambda I}(t) \sim 0$ from [2], and

$$\hat{\epsilon}_{\lambda S}(t) \rightarrow \hat{\epsilon}_{\lambda S} \equiv (1 - r_{\lambda FS})\,(1 - r_{\lambda SF}) \qquad [8]$$

from [3]. Note that $\hat{\epsilon}_{\lambda S}$ is then time-independent. Putting these results into [1], we have

$$I_{\lambda mod}(\lambda,t) \rightarrow I_{\lambda mod}(\lambda) \approx (1 - r_{\lambda FS})(1 - r_{\lambda SF})\, I_{\lambda pl}(\lambda,T_s) = \hat{\epsilon}_{\lambda S}\, I_{\lambda pl}(\lambda,T_s) \qquad [9]$$

which represents a constant radiation intensity at a given wavelength, just we observed in the data (Figures 2 and 3). The minimum values of $a_{\lambda S}$ required by the condition $a_{\lambda S} \gtrsim 1/(d-v_s t_{exp})$ may be calculated from the experimental parameters listed in Table IV. We list the results of this calculation in Table IV, where we see that, for crystal Di, $a_{\lambda S} \gtrsim 700$–$1100\ m^{-1}$, while for glass Di, we have $a_{\lambda S} \gtrsim 420\ m^{-1}$.

As the shock wave reaches the free surface of the unshocked sample (t_s in Figure 2 or 3), the radiation radiation intensity again becomes transient, and the experiment is over. Since we want to infer the shock-compressed temperature of the sample from the shock-induced sample radiation, and since [9] is most likely valid for $t \approx t_{exp}$, we use the magnitude of the radiation intensity at t_{exp} (Table IV, just prior to t_s, Figure 2 or 3) and each wavelength to constrain the temperature of the shocked sample. Assuming the spectral reflectivities $r_{\lambda FS}$ and $r_{\lambda SF}$ are independent of wavelength, [9] is analogous to the greybody relation, *i.e.*,

$$I_{\lambda gb}(\lambda,t_{exp}) \equiv \hat{\epsilon}_{fit}(t_{exp})\, I_{\lambda pl}(\lambda,T_{fit}) \qquad [10]$$

Comparing [9] and [10], we see that $\hat{\epsilon}_{fit}(t_{exp})$ should constrain the value of $(1-r_{\lambda FS})(1-r_{\lambda SF})$. The value of t_{exp} reflects the calculated shock-wave transit time through the sample, but is not critically dependent on this choice (Svendsen and Ahrens, 1987) as long as the optical parameters of the unshocked material (*e.g.*, $a_{\lambda US}$) are not strongly wavelength dependent. At t_{exp}, then we measure the spectral radiance at 4 wavelengths (450, 600, 750 and 900 nm), and we may fit

$I_{\lambda gb}(\lambda,t_{exp})$ to this data via the χ^2 statistic (*e.g.*, Press *et al.*, 1986). In this case, it is given by

$$\chi^2(t_{exp}) \equiv \chi^2[t_{exp};\hat{\epsilon}_{fit},T_{fit}]$$

$$\equiv \sum_{\lambda}\left\{ \frac{1}{[\sigma(\lambda)]^2} \{ I_{\lambda exp}(\lambda,t_{exp}) - \hat{\epsilon}_{fit}(t_{exp})\, I_{\lambda pl}[\lambda,T_{fit}(t_{exp})] \}^2 \right\} \quad . \quad [11]$$

where $\sigma(\lambda)$ are the experimental uncertainties at each wavelength. On this basis, $\hat{\epsilon}_{exp}(t_{exp})$ and $T_{exp}(t_{exp})$ represent the values of $\hat{\epsilon}_{fit}(t_{exp})$ and $T_{fit}(t_{exp})$ that minimize $\chi^2(t_{exp})$; in light of [8] and [9], this implies that $\hat{\epsilon}_{exp} = \hat{\epsilon}_{\lambda s}$ and $T_{exp} = T_s$. Since the fit is an average over λ, the value of $\hat{\epsilon}_{exp}$ represents a λ-average of $\hat{\epsilon}_{\lambda s}$. Since χ^2 is a nonlinear functional of temperature, we find its minimum numerically using 1) Golden section (GS) search, and 2) the method of Levenberg as formulated by Marquardt (LM). See, for example, Press *et al.* (1986), for details on both of these methods. To obtain starting values of $\hat{\epsilon}_{fit}(t)$ and $T_{fit}(t)$ for the nonlinear fit, we use Wien's approximation to $I_{\lambda pl}(\lambda,T)$ in $\chi^2(t_{exp})$ which follows from $I_{\lambda pl}(\lambda,T)$ in the limit $\exp(C_2/\lambda T) \gg 1$, *i.e.*,

$$I_{\lambda wgb}(\lambda,t) \equiv \hat{\epsilon}_{fit}(t)\, I_{\lambda wi}(\lambda,t) = \hat{\epsilon}_{fit}(t)\, \frac{2C_1}{\lambda^5}\, e^{-C_2/\lambda T_{fit}(t)} \quad . \quad [12]$$

We fit Wien's relation to the data via linear least-squares, and solve for $\hat{\epsilon}_{fit}(t_{exp})$ and $T_{fit}(t_{exp})$.

We present the results of the greybody fit for the six experiments in Table II, and we plot these results in Figures 3a-c. We note that, with 3 or 4 data points and 2 parameters in each of these fits, a χ^2 value of $\sim$2 is representative of a "good" fit; this value is very sensitive to measurement uncertainties, as can be seen from [10]. In this case, the values of χ^2 in Table II imply that we may have overestimated measurement uncertainties. Also, note that T_{exp} is much less sensitive to uncertainties than $\hat{\epsilon}_{exp}$, given the form of $I_{\lambda gb}$ (Svendsen and Ahrens, 1987). In Table II, the uncertainties quoted with the GS fits represent measurement uncertainties mapped into uncertainties for $\hat{\epsilon}_{exp}(t_{exp})$ and $T_{exp}(t_{exp})$ (Boslough *et al.*, 1986). However, the uncertainty quoted with each LM fit is the

standard deviation of that fit. Note that the GS and LM fits for shot 196, and the Wien, GS and LM fits for shot 197, give $\hat{\epsilon}_{exp}$ well above unity, which is an unphysical result. As noted by Boslough *et al.* (1986), however, $\hat{\epsilon}_{fit}$ is much more sensitive to data scatter, whether due to uncorrected λ-dependences in the data, or experimental measurement errors. As can be seen from the corresponding GS fits where $\hat{\epsilon}_{fit}$ is set equal to one, the variable $\hat{\epsilon}_{fit}$ fits for shots 196 and 197 may then underestimate the value of T_{exp} by $\sim$200 K. Also note that the value of $\hat{\epsilon}_{exp}$ for all experiments and all fits is $\gtrsim$0.1, which implies that we are observing relatively homogeneous radiation from the sample, as opposed to localized, "shear-band" radiation seen in many shock-compressed oxides and silicates at lower ($\lesssim$ 70 GPa) pressure (*e.g.*, Kondo and Ahrens, 1983; Schmitt *et al.*, 1986). Although the constraint is very poor, we note that, from the identification $(1-r_{\lambda FS})(1-r_{\lambda SF})\approx\hat{\epsilon}_{exp}$, as discussed above, $r_{\lambda SF}\sim$0.1 with $r_{\lambda FS}\sim$0.1, for shots 140 and 141, at least.

Hugoniot Calculations and Comparison with Data

We calculate the density, ρ_H, and pressure, P_H, of the shock-compressed Di states, from an impedance match (Rice *et al.*, 1958) between the target components assuming a linear shock velocity, U, material velocity, v, relation, *i.e.*, $U = a_i + b_i v$. For Ta, we use ρ_i^{α}=16675 kg/m^3, a_i=3290 m/s and b_i=1.31 (Mitchell and Nellis, 1984), while for Ag, we use ρ_i^{α}=10501kg/m^3, a_i=3270 m/s and b_i=1.55 (Marsh, 1980). We assume the U-v relation for crystal Di, which is experimentally-constrained to 100 GPa (Svendsen and Ahrens, 1983) is valid to 170 GPa (Table III). Since there are no U-v data for glass Di, we must estimate the U-v coefficients for glass Di, a_{ig} and b_{ig}, from those of the corresponding crystal material, a_{ic} and b_{ic}. With a_{ig} and b_{ig}, we may calculate the impedance match for glass Di targets, and so estimate the experimental glass Di Hugoniot states. Since the U-v relation represents a Taylor's series expansion of U(v) about the initial state v=0, a_i and b_i are defined by

$$a_i \equiv \lim_{v \to 0} \left\{ U^2 \right\}^{1/2} \quad [13]$$

$$b_i \equiv \lim_{v \to 0} \left\{ \frac{dU}{dv} \right\} \quad [14]$$

Now, we may connect U and v to P_H via the relations

$$U^2 = \frac{1}{\rho_i^{\alpha} \eta_H} [P_H - P_i] \quad [15]$$

and

$$v^2 = \frac{\eta_H}{\rho_i^{\alpha}} [P_H - P_i] \quad [16]$$

Using [13] and [14] in [15] and [16], and noting that the limit $\rho_H \to \rho_i^{\alpha}$ is equivalent to $v \to 0$, we obtain

$$a_i = \left\{ \lim_{\rho_H \to \rho_i^{\alpha}} \left\{ \frac{dP_H}{d\rho_H} \right\} \right\}^{1/2} \quad [17]$$

and

$$b_i = \frac{1}{4} \left\{ 1 + \lim_{\rho_H \to \rho_i^{\alpha}} \left\{ \frac{d\ln B_H}{d\ln \rho_H} \right\} \right\} \quad [18]$$

with

$$B_H \equiv \rho_H \left\{ \frac{dP_H}{d\rho_H} \right\} \quad [19]$$

We relate glass and crystal Di Hugoniot states at the same density, occupying the same phase, via the relation (Svendsen, 1987)

$$P_{gH}(\rho_H) = \frac{(1-\phi)[1-(1+\frac{1}{2}\gamma_H)\eta_{cH}]}{[1-(1+\frac{1}{2}\gamma_H)\eta_{gH}]} P_{cH} + \gamma_H \frac{\frac{1}{2}\phi P_i + \rho_{ig}^{\alpha} \Delta e_i^{c-g}}{[1-(1+\frac{1}{2}\gamma_H)\eta_{gH}]} \quad [20]$$

Relation [20] depends on the assumption that γ, the equilibrium thermodynamic Grüneisen's parameter, is a function of density alone. In [20], we have $\gamma_H \equiv \gamma(\rho_H)$, $\eta_{gH} \equiv 1 - \rho_{ig}^{\alpha}/\rho_H$ is the relative compression of the glass, $\eta_{cH} \equiv 1 - \rho_{ic}^{\alpha}/\rho_H$ is the relative compression of the crystal, $\phi \equiv 1 - \rho_{ig}^{\alpha}/\rho_{ic}^{\alpha}$ is the

"porosity," and $\Delta e_i^{c-g} \equiv e(\rho_{ic}^{\alpha}, s_{ic}^{\alpha}) - e(\rho_{ig}^{\alpha}, s_{ig}^{\alpha})$ is the difference in specific internal energy between the glass and crystal in the low pressure phase at T_i and P_i. Further, P_{gH} is the pressure of the glass Hugoniot state, P_{cH} is the pressure of the crystal Hugoniot state, ρ_{ig}^{α} and s_{ig}^{α} are the initial glass density and specific entropy, and ρ_{ic}^{α} and s_{ic}^{α} are the initial crystal density and specific entropy. Since relations [13]-[19] are valid for any "hydrodynamic" starting material, we have

$$a_{ig} = \lim_{\rho_H \to \rho_{ig}^{\alpha}} \left(\frac{dP_{gH}}{d\rho_H} \right)^{1/2} \qquad [21]$$

$$b_{ig} = \frac{1}{4} \left\{ 1 + \lim_{\rho_H \to \rho_{ig}^{\alpha}} \left\{ \left(\frac{d\ln B_{gH}}{d\ln \rho_H} \right) \right\} \right\} \qquad [22]$$

for glass Di, with P_{gH} given by [20]. Note that [19] relates the density derivatives of P_{gH} to those of P_{cH}, which we obtain from (McQueen *et al.*, 1967)

$$P_{cH} = P_i + \frac{\rho_{ic}^{\alpha} a_{ic}^2 \eta_{cH}}{(1 - b_{ic}\eta_{cH})^2} \qquad [23]$$

the so-called shock wave equation-of-state. So, via [20]-[23], we may calculate a_{ig} and b_{ig} as functions of ρ_{ig}^{α}, ρ_{ic}^{α}, a_{ic} and b_{ic}. These then allow us to calculate an impedance match for targets containing glass Di as the sample material, and obtain an estimate of the glass Di P_H, ρ_H state. We also use [20] to estimate the $\rho_H(P_{gH})$ and so $T_H(P_{gH})$ via [24] below.

The temperature of a singly shock-compressed material, T_H, may be estimated from an equilibrium thermodynamic energy balance (*e.g.*, McQueen *et al.*, 1967; Ahrens *et al.*, 1969; Jeanloz and Ahrens, 1980b; see Svendsen, 1987, for details) in which we assume the material compresses adiabatically, and as an elastic fluid. On this basis, if we compress a material from an initial state (P_i, T_i) to a shock-compressed state (P_H, T_H), assuming the material undergoes a phase transition from a low pressure phase, α, to a high pressure phase, β, the Hugoniot temperature of the β-phase, T_H, may be written

$$T_H = T_{s_i} + \frac{1}{c_V} \left\{ \frac{1}{2} \left\{ \frac{1}{\rho_i^{\alpha}} - \frac{1}{\rho_H} \right\} P_H - [\Delta e_{s_i} + \Delta e_i^{\alpha-\beta}] \right\} \qquad [24]$$

with $\eta_H \equiv 1-\rho_i^\alpha/\rho_H$ being the relative compression. To write [24], we assume that c_v, the specific heat at constant volume of the shock-compressed state, is independent of temperature, which is justified *a posteriori* by our results below. The subscripts "i", "H", "S" and "V" designate initial, shock-compressed, constant entropy and constant volume states of the material, respectively. Note that all quantities in [24], and the expressions to follow, apply to the high-pressure phase, β, unless otherwise designated. In [24], $\Delta e_i^{\alpha-\beta}$ is the difference in specific internal energy between the two phases at T_i and P_i, Δe_{s_i} is the change in specific internal of β compressed isentropically (at specific entropy s_i) from its density at STP, ρ_i, to a density ρ_H (that of the shock-compressed state), while T_S is the temperature of the material along the isentrope referenced to s_i and ρ_i. Also, P_H is the pressure of the shock-compressed state.

The temperature, T_{s_i}, along the compression isentrope may be estimated from γ via the relation

$$T_{s_i} = T(s_i,\rho_H) \equiv T_i \exp\left\{\gamma(\rho_i)\left[1-\frac{\rho_i}{\rho_H}\right]\right\} . \qquad [25]$$

since we assume $\gamma\rho$ is constant in all model calculations. Lastly, we estimate Δe_{s_i} from the same energy balance used to obtain [24], the expression for T_H (Svendsen, 1987).

Since we usually have values for ρ_{ig}^α, ρ_{ic}^α, a_{ic} and b_{ic} *a priori*, and we can estimate a_{ig} and b_{ig} as discussed above, we use these to calculate impedance matches for targets containing crystal and glass Di. The impedance match gives us ρ_{cH},P_{cH} and ρ_{gH},P_{gH}. With these, we have $T_{cH}(P_{cH})$ and $T_{gH}(P_{gH})$ from [24], given estimates of ri, γ and c_v for β, as well as $\Delta e_i^{\alpha-\beta}$ ($\Delta e_i^{\alpha-\beta}+\Delta e_i^{c-g}$ for the glass). Requiring $P_{gH}\rightarrow P_i$ as $\rho_H\rightarrow\rho_{ig}^\alpha$, we have Δe_i^{c-g} from [20], *i.e.*,

$$\Delta e_i^{c-g} = \frac{1}{\rho_{ig}^\alpha\gamma_{ig}}\left\{(1-\tfrac{1}{2}\gamma_{ig}\phi)P_i - (1-\phi)[1-(1+\tfrac{1}{2}\gamma_{ig})\eta_{cg}]P_{cH}(\rho_{ig}^\alpha)\right\}$$

with $\eta_{cg}\equiv 1-\rho_{ic}^\alpha/\rho_{ig}^\alpha$ and $\gamma_{ig} \equiv \gamma(\rho_{ig}^\alpha)$. In this case, T_H for glass and crystal Di starting materials depends on the basic unknowns ρ_i, γ and c_v for the high-

pressure phase, β, as well as $\Delta e_i^{\alpha-\beta}$. From [24], we see that the slope of $T_H(P_H)$ is controlled by the magnitude of c_v, while the initial value of T_H is governed by $\Delta e_i^{\alpha-\beta}$. Further, from [24] and [25], we see that γ influences T_H via the isentropic properties T_{s_i} and Δe_{s_i}. In addition, γ influences the Hugoniot temperature of glass Di through [20]. The density of β at T_i and P_i, ρ_i, influences T_H indirectly, but significantly, through [24], [25], and $\gamma(\rho)$.

In Figures 4a-c, we display calculated Hugoniots for crystal and glass Di that "fit" the shock temperatures constrained by the data discussed above. We give a range of these Hugoniots based on a range of values for ρ_i (3900-4300 kg/m^3, Figure 4a), $\gamma_i = \gamma(\rho_i)$ (1-2, Figure 4b), and $\Delta e_i^{\alpha-\beta}$ (0.4-1.4 MJ/kg for crystal Di, and 1.8-2.8 MJ/kg for glass Di, Figure 4c) to demonstrate the sensitivity of T_H to these unknowns. In all these calculations, we assume that c_v is given by its classic lattice value, $3\nu R/M$ (Table III). The experimental results for the slope of $T_H(P_H)$ for the crystal and glass Di Hugoniots suggest this is not an unreasonable assumption, although there are not enough data to rule out a pressure-temperature dependent c_v (*e.g.*, Lyzenga *et al.*, 1983; Boslough *et al.*, 1986). From previous work on the pressure-density Hugoniot of Di (Ahrens *et al.*, 1966; Svendsen and Ahrens, 1983), the range of possible ρ_i values shown in Figure 4a for HPP Di are based on mixed-oxide and perovskite models for HPP Di. Comparing the results in these figures, we see that T_H for crystal Di is most sensitive to ρ_i, followed by $\Delta e_i^{\alpha-\beta}$ and then γ_i. For glass Di, T_H may be slightly more sensitive to γ_i than $\Delta e_i^{\alpha-\beta}$, but not really knowing a plausible range of values for these parameters, it is hard to say.

From the curves in Figures 4a and 4c, we note that the glass data would also be satisfied by the combination of a lower initial density (3900 kg/m^3) and lower value of $\Delta e_i^{\alpha-\beta}$ (1.8 MJ/kg); this is also consistent with the glass Di states representing liquid. Even if $\rho_i \approx 4100$Mk/kg for glass Di, melting is favored, considering the magnitude of $\Delta e_i^{\alpha-\beta}$ (2.3 MJ/kg) needed to "fit" this data. The magnitude of $\Delta e_i^{\alpha-\beta}$ for the "best-fit" crystal Di Hugoniot (0.8 MJ/kg, Table III)

is of the same order as those estimated for some silicate and oxide dynamic solid-solid phase transformations (*e.g.*, 0.82 MJ/kg, α–SiO_2→stishovite, Lyzenga *et al.*, 1983). If the glass data represent a solid-solid plus melting transition, this implies a value for $\Delta e_i^{\alpha-\beta}$ of $\approx$ 1.5 MJ/kg for melting of HPP Di. This compares, for example, with 1.6 MJ/kg estimated by Lyzenga *et al.* (1983) for the stishovite→liquid SiO_2 transition. This line of thought also leads us to believe that the glass Di data represent liquid Di, while the crystal Di data represent a mixture of high-pressure oxide (B2-CaO, MgO plus stishovite) and/or perovskite ($CaSiO_3$ plus $MgSiO_3$, or $CaSiO_3$ - $MgSiO_3$ solid solution) phases.

Discussion

In Table IV, we list the greybody fit and uncertainties, along with the calculated shock-wave velocities, shock-transit times, pressure and temperature, for each experiment. The values of $\hat{\epsilon}_{exp}(t_{exp})$ and $T_{exp}(t_{exp})$ in Table IV for shots 140, 141, 169 and 170 are those for the GS fit with $\hat{\epsilon}_{fit}$ and T_{fit} variable, which we choose as representative of the other estimates, within experimental uncertainties. As discussed above, since $\hat{\epsilon}_{exp}(t_{exp})$ for shots 196 and 197 are significantly greater than unity, we choose the GS fit with $\hat{\epsilon}_{fit}$ set to one as the "experimental results" for these shots as listed in Table IV.

We display the "best fit" Hugoniot to the present experimental results (continuous curve) in Figure 5 along with other experimental results inferred from radiation data for SiO_2 (Lyzenga *et al.*, 1983), CaO (Boslough *et al.*, 1986), and MgO (Svendsen & Ahrens, 1987). Also shown are the mantle temperature profiles of Brown & Shankland (1980) and Stacey (1977). These two models represent the range of models currently considered plausible. The HPP Di results fall between the CaO and MgO results, and well-below those for stishovite and liquid-SiO_2. To first order, this is due to the differences in the STP densities of the HPP's of each material. MgO, which apparently does not undergo any phase transformation below 200 GPa (Vassiliou and Ahrens, 1981; Svendsen and Ahrens, 1987) has an STP density of 3583 kg/m^3, B2-CaO has an initial density of $\approx$ 3800-4000 kg/m^3 (Jeanloz and Ahrens, 1980a; Boslough *et al.*, 1984), HPP solid Di is likely to have a slightly larger ρ_i ($\approx$4100 kg/m^3, Table III) than B2-CaO, as discussed above, and stishovite has an STP density of $\approx$ 4300 kg/m^3. This is also true because the values of $\Delta e_i^{\alpha-\beta}$ for each material are approximately the same. Since B2-CaO and HPP Di apparently have very similar ρ_i, other factors, such as compressibility (B2-CaO has a lower bulk modulus than HPP Di: Jeanloz and Ahrens, 1980a; Boslough *et al.*, 1983; Svendsen and Ahrens, 1983), become important. B2-CaO is more compressible than HPP Di, and so its Hugoniot temperature rises more quickly than HPP Di.

Low pressure static studies of Di (*e.g.*, Liu, 1979b) imply that $CaMgSi_2O_6$ may disproportionate into $CaSiO_3$ perovskite and $MgSiO_3$ perovskite above $\approx$ 20 GPa and 1000 C. Our results are not inconsistent with this, and yet we really cannot distinguish between perovskite and mixed-oxide (or some combination) assemblage. The model we favor (Table III) is more likely representative of the perovskite mixture for $CaMgSi_2O_6$ (Svendsen and Ahrens, 1983).

In comparison with the mantle temperature profiles displayed in Figure 5, we note that both B2-CaO and HPP Di Hugoniot may be at about the same temperature at the pressures of the lowermost mantle. We note that some of the compositional models for the lowermost mantle (*e.g.*, Ruff and Anderson, 1980), known as the D" region, contain significant amounts of more refractory oxides and/or silicates (*i.e.*, CaO, Al_2O_3, $CaSiO_3$, *etc.*.).

Summary

Observed radiation from shock-compressed crystal $CaMgSi_2O_6$ (Di) constrains Hugoniot temperatures of 3500-4800 K for this material in the 150-170 GPa pressure range, while glass $CaMgSi_2O_6$, with a starting density 87% that of crystal Di, achieves Hugoniot temperatures of 3600-3800 K in the 105-107 GPa pressure range. The shock-induced radiation history for these materials implies that both shock-compressed crystal and glass Di are strong absorbers ($a_{\lambda s} \gtrsim$500–1000 m^{-1}). Calculated Hugoniot states for these materials, in comparison with the experimental results, suggest that crystal Di Hugoniot states in the 150-170 GPa range represent a HPP solid (or possibly liquid) phase with an STP density of 4100$\pm$200 kg/m^3, STP Grüneisen's parameter of 1.5$\pm$0.5 and STP HPP-LPP specific internal energy difference of 0.9$\pm$0.5 MJ/kg. These parameters are consistent with either a Ca-Mg mixed-oxide or pervoskite assemblage. For glass Di, we have the same range of HPP properties, except that $\Delta e_i^{\alpha-\beta}$ is 2.3$\pm$0.5 MJ/kg, a strong indication that the glass Di Hugoniot states occupy the liquid-phase of $CaMgSi_2O_6$, and that $\Delta e_i^{\alpha-\beta} \approx$1.5Mg/kg for HPP-Di

melting. This value for $\Delta e_i^{\alpha-\beta}$ is similar to the shock temperature results for SiO_2 (Lyzenga *et al.*, 1983). Comparison of the experimentally-constrained pressure-temperature Hugoniot of crystal Di with the experimentally-constrained Hugoniots of its constituent oxides (*i.e.*, SiO_2, CaO and MgO) demonstrates the strong influence of the HPP, STP density of these materials on the magnitude of the temperature in their shock-compressed states. The experimentally-constrained crystal Di Hugoniot falls within the plausible range (2500-3000 K) of mantle temperature profiles in the range of pressures (110-135 GPa) corresponding to the lowermost mantle.

Acknowledgements. We thank Papo Gelle, Mike Long, Chuck Manning and Leon Young for experimental assistance, and Gregory Miller, Jay D. Bass, Douglas R. Schmitt and James A. Tyburczy for enlightening discussions. Support under NASA and NSF grants NGL-05-002-105 and EAR-86-08249, respectively, is gratefully acknowledged. Contribution 4480, Division of Geological and Planetary Sciences, California Institute of Technology, Pasadena, California.

References

Ahrens, T. J., J. T. Rosenburg and M. H. Ruderman, Dynamic properties of rocks, *Standford Research Institute, Final Report*, DA-45-146-XZ-277, SRI Project FGU-4816, Sept. 1966.

Ahrens, T. J., Anderson, D. L. and Ringwood, A. E., 1969. Equation of state and crystal structure of high-pressure phases of shocked silicates and oxides, *Rev. Geophys., 37*, 667-707.

Bass, J. D., Svendsen, B. and Ahrens, T. J., 1987. The temperatures of shock-compressed iron, *High Pressure Research in Geophysics and Geochemistry*, eds. M. Manghnani and Y. Syono, American Geophysical Union, in press.

Binsted, N., Greaves, G. N., and C. M. B. Henderson, 1985. An EXAFS study of glassy and crystalline phases of compositions $CaAl_2Al_2Si_2O_8$ and $CaMgSi_2O_6$, *Contrib. Mineral. Petrol., 89*, 103-109.

Boslough, M. B., 1984. Shock-wave properties and high-pressure equations-of-state of geophysically-important materials, *Ph.D. dissertation*, California Institute of Technology, Pasadena, California, 171 pp.

Boslough, M. B., 1985. A model for time dependence of shock-induced thermal radiation of light, *J. appl. Phys., 56*, 3394-3399.

Boslough, M. B., Ahrens, T. J. and Mitchell, A. C., 1984. Shock temperatures in CaO, *J. Geophys. Res., 89*, 7845-7851.

Boslough, M. B., Ahrens, T. J. and Mitchell, A. C., 1986. Shock temperatures in anorthite glass, *Geophys. J. R. astr. Soc., 84*, 475-489.

Brown, J. M. and Shankland, T., 1980. Thermodynamic parameters of the Earth as determined from seismic profiles, *Geophys. J. R. astr. Soc., 66*, 579-596.

Grossman, L. and Larimer, J. W., 1974. Early chemical history of the solar system, *Rev. Geophys. Space Phys., 12, 71-101.*

Grover, R. and Urtiew, P. A., 1974. Thermal relaxation at interfaces following shock compression, J. appl. Phys., 45, 146-152.

Jeanloz, R. and Ahrens, T. J., 1980a. Equations of state of FeO and CaO, *Geophys. J. R. astr. Soc., 62*, 505-528.

Jeanloz, R. and Ahrens, T. J., 1980b. Anorthite: thermal equation of state to high pressures, *Geophys. J. R. astr. Soc., 62*, 529-549.

Kondo, K. E. and Ahrens, T. J., 1983. Heterogeneous shock-induced thermal radiation in minerals, *Phys. Chem. Minerals, 9*, 173-181.

Kormer, S. B., 1968. Optical study of the characteristics of shock-compressed condensed dielectrics, *Sov. Phys. Uspekhi, 11*, 229-254.

Liu, L. G., 1978. A new high-pressure phase of $Ca_2Al_2SiO_7$ and implications for the Earth's interior, *Earth Planet. Sci. Lett., 40*, 401-406.

Liu, L. G., 1979a. High-pressure phase transformations in the system $CaSiO_3$–Al_2O_3, *Earth Planet. Sci. Lett., 43*, 331-335.

Liu, L. G., 1979b. The system enstatite-wollastonite at high pressures and temperatures, with emphasis on diopside, *Phys. Earth Planet. Int., 19*, P15-P18.

Lyzenga, G. A., 1980. Shock Temperatures of Materials: Experiments and Applications to the High Pressure Equation of State, *Ph.D. Dissertation*, California Institute of Technology, Pasadena, California, 201 pp.

Lyzenga, G. A., Ahrens, T. J. and Mitchell, A. C., 1983. Shock temperatures of SiO_2 and their geophysical implications, *J. Geophys. Res., 88*, 2431-2444.

Marsh, S. P., 1980. *LASL shock Hugoniot data*, University of California Press, Los Angeles, CA, 658 pp.

McQueen, R. G., S. P. Marsh and J. N. Fritz, 1967. Hugoniot equation of state of twelve rocks, *J. Geophys. Res.* 72:4999-5036.

Mitchell, A. C. and W. J. Nellis, 1984. Shock compression of aluminum, copper and tantalum, *J. Appl. Phys., 52*, 3363-3374.

Press, W. H., B. P. Flannery, S. A. Teukolsky and W. T. Vetterling, *Numerical Recipies: The Art of Scientific Computing,*, Cambridge University Press, New York, NY, 818 pp. (1986).

Rice, W. H., R. G. McQueen and J. M. Walsh, 1958. Compressibility of solids by strong shock waves, *Solid State Phys., 6,*, pp. 1-63.

Robie, R. A., B. S. Hemingway and R. J. Fisher, *Thermodynamic properties of minerals and related substances at 298.15 K and 1 bar (10^5 Pascals)*

pressure and at higher temperatures, USGS Bulletin 1452, Government Printing Office, Washington, D.C., 456 pp.

Ruff, L. J. and D. L. Anderson, 1980. Core formation, evolution and convection: a geophysical model, *Phys. Earth Planet. Int., 21,* 181-201.

Ruoff, A. L., 1967. Linear shock velocity-particle velocity relation, *J. Appl. Phys., 38,* 4976-4980.

Schmitt, D. R., Svendsen, B. and Ahrens, T. J., 1986. Shock-induced radiation from minerals, in *Shock waves in condensed matter - 1985*, pp. 261-266, ed. Y. M. Gupta, Plenum Press, New York, NY.

Stacey, F., 1977. A thermal model of the Earth, *Phys. Earth Planet. Int.*, **15**, 341-348.

Svendsen, B, Optical radiation from shock-compressed materials, *Ph.D. dissertation*, California Institute of Technology, 250 pp., (1987).

Svendsen, B. and T. J. Ahrens, 1983. Dynamic compression of diopside and salite to 200 GPa, *Geophys. Res. Lett., 7,* 501-504.

Svendsen, B. and T. J. Ahrens, 1987. Shock-induced temperatures of MgO, *Geophys. J. R. astr. Soc.*, in press.

Turekian, K. K. and S. P. Clark (Jr.), 1969. Inhomogeneous accretion model of the Earth from the primitive solar nebula, *Earth planet. Sci. Lett., 6,* 346-348.

Urtiew, P. A. and Grover, R., 1974. Temperature deposition caused by shock interactions with material interfaces, *J. Appl. Phys., 45,*, 140-145.

Table I. Microprobe Analyses of Starting Materials.

Shot	140,141†	169,170‡	196,197§
Na_2O	0.38*	0.48	0.39
MgO	17.40	17.63	17.59
Al_2O_3	0.36	0.22	0.36
SiO_2	55.74	55.32	56.08
CaO	25.15	24.78	25.30
TiO_2	0.02	0.11	0.02
Cr_2O_3	0.07	0.48	0.02
MnO	0.08	0.04	0.06
FeO	0.82	0.96	0.81
Total	99.97	99.68	100.63
En	48.4	49.0	48.4
Wo	50.3	49.5	50.3
Fs	1.4	1.5	1.4

† Diopside from DeKalb, NY, supplied by S. Huebner, USGS, Reston, VA.

‡ Russian diopside, supplied by Gem Obsessions, San Diego, CA.

§ Diopside glass, supplied by G. Miller, Caltech, and G. Fine, Corning Glass Co.

* wght. %

Table II. Radiation data and fits.

Spectral Radiance ($kW/m^2 \cdot sr \cdot nm$)					Fits				
Shot	450 (nm)	600 (nm)	750 (nm)	900 (nm)	Parameter(t_r)	Wien	GS†	LM‡	GS ($\hat{\epsilon}_{fit}$=1)
140		3.15	3.09	2.87	$\hat{\epsilon}_{exp}$(140 ns)	0.65	0.59	0.56	
		(0.59)	(0.45)	(0.81)		(0.37)	(0.37)	(0.23)	
					T_{exp}(140 ns)	4152	4215	4270	3803
						(351)	(364)	(356)	(293)
					χ^2	0.14	0.06	0.06	0.05
141	6.14	5.38	6.06	5.71	$\hat{\epsilon}_{exp}$(145 ns)	0.71	0.65	0.75	
	(1.21)	(1.00)	(0.77)	(0.93)		(0.34)	(0.34)	(0.11)	
					T_{exp}(145 ns)	4737	4782	4643	4372
						(346)	(356)	(153)	(297)
					χ^2	3.44	3.13	3.05	3.55
169	5.11	6.58	6.53	5.49	$\hat{\epsilon}_{exp}$(198 ns)	0.91	0.86	0.86	
	(0.18)	(0.31)	(0.33)	(0.31)		(0.27)	(0.27)	(0.18)	
					T_{exp}(198 ns)	4522	4552	4555	4428
						(263)	(268)	(178)	(251)
					χ^2	0.30	0.21	0.21	0.48
170	0.82	1.56	2.34	2.29	$\hat{\epsilon}_{exp}$(170 ns)	1.01	1.04	1.06	
	(0.13)	(0.17)	(0.26)	(0.26)		(0.25)	(0.25)	(0.17)	
					T_{exp}(170 ns)	3539	3508	3498	3539
						(143)	(141)	(90)	(143)
					χ^2	1.61	1.43	1.42	1.52
196	1.35	2.14	2.96	3.24	$\hat{\epsilon}_{exp}$(485 ns)	1.09	1.23	1.63	
	(0.48)	(0.33)	(0.42)	(0.51)		(0.44)	(0.44)	(0.26)	
					T_{exp}(485 ns)	3695	3585	3422	3711
						(243)	(231)	(100)	(247)
					χ^2	1.99	1.20	1.03	1.72
197	1.37	3.18	3.46	3.74	$\hat{\epsilon}_{exp}$(475 ns)	1.51	1.51	1.38	
	(0.41)	(0.39)	(0.50)	(0.56)		(0.39)	(0.39)	(0.22)	
					T_{exp}(475 ns)	3610	3610	3663	3866
						(208)	(208)	(96)	(239)
					χ^2	0.50	0.50	0.46	1.23

† - Golden section search fit. Uncertainties represent experimentally-based uncertainties, and this fit is unweighted.

‡ - Levenberg-Marquardt fit. Uncertainties represent standard deviations of corresponding fit, and this is a weighted fit.

Table III. $CaMgSi_2O_6$ STP parameters.

Property	Symbol	crystal	glass	Units
		U-v relation†		
Density	ρ	3277[a]	2828[b]	kg/m^3
Intercept	a	5620[c]	4775[d]	m/s
Slope	b	1.27[c]	1.28[d]	
		High-pressure phase		
Density	ρ	4100[c]	4100[c]	kg/m^3
Intercept	a	7826[e]	7826[e]	m/s
Slope	b	1.22[e]	1.22[e]	
Bulk modulus	K_s	251[f]	251[f]	GPa
$(\partial K_s/\partial P)_s$	K_s'	3.90[g]	3.90[g]	
Grüneisen's parameter‡	γ	1.5[h]	1.5[h]	
Specific heat§	c_v	1151.8	1151.8	J/kg·K
HPP-LPP energy difference	$\Delta e_i^{\alpha-\beta}$	0.9[h]	2.3[h]	MJ/kg

†*i.e.*, U=a+bv. These relations are valid for v>2000 m/s.

‡ $\rho\gamma$=constant assumed in all calculations.

§ Dulong-Petit value, used for c_v in all calculations.

[a] Robie *et al.* (1978).
[b] Table IV.
[c] Svendsen & Ahrens (1983).
[d] from method discussed in text.
[e] U-v relation referenced to STP density of HPP (Svendsen, 1987).
[f] calculated assuming $K_s = \rho a^2$.
[g] calculated with $(\partial K_s/\partial P)_s = 4b-1$ (Ruoff, 1967).
[h] from model calculations discussed in text.

Table IV. Experimental results and model estimates.

Shot	Experimental Results					Calculated Results					
	ρ (kg/m^3)	d (mm)	v_{im} (m/s)	$\hat{\epsilon}_{exp}$	T_{exp} (K)	U (m/s)	v (m/s)	$a_{\lambda ss}$ (m^{-1})	t_{st} (ns)	P_H (GPa)	T_H (K)
140	3282 (6)†	1.868 (0.010)	5983 (60)	0.57 (0.23)	4215 (364)	11210	4403	880	167	162	4190
141	3283 (6)	1.566 (0.010)	6143 (50)	0.90 (0.20)	4782 (356)	11360	4518	1061	140	169	4524
169	3290 (5)	2.424 (0.004)	6048 (40)	0.97 (0.24)	4555 (268)	11300	4448	681	192	165	4313
170	3289 (7)	1.970 (0.010)	5593 (50)	0.85 (0.14)	3508 (141)	10850	4121	818	182	147	3590
196	2829 (1)	4.008 (0.004)	4673 (30)	1.00 (0.44)	3711 (231)	9678	3884	417	414	105	3660
197	2827 (1)	3.966 (0.001)	4729 (30)	1.00 (0.39)	3866 (208)	9733	3885	420	408	107	3795

† - measurement uncertainty.

ρ - STP bulk density.

d - Sample thickness.

v_{im} - Impact velocity.

$\hat{\epsilon}_{exp}$ - Experimentally-constrained greybody effective emissivity.

T_{exp} - Experimentally-constrained greybody absolute temperature.

t_r - Time during radiation history when I_{exp} used to constrain T_{exp} and $\hat{\epsilon}_{exp}$ was read.

U - Calculated shock wave velocity through sample.

v - Calculated material velocity of shocked sample sample.

$a_{\lambda ss}$ - lower bound to absorption coefficient of shocked sample.

t_{st} - Calculated shock wave transit time through sample.

P_H - Calculated shock-compressed pressure of sample.

T_H - Calculated shock-compressed temperature of sample.

Figure captions

Figure 1. Geometry of the light-gas gun radiation experiment after Boslough (1984). The projectile, shot through the barrel, impacts the sample at velocities between 4.6 and 6.1 km/sec. Radiation from the sample is turned 90° by the mirror, travels through the objective lens, and is divided up by the three beam-splitter arrangement among the 4 channels of the pyrometer. The resulting signals from the photodiode in each channel are monitored by oscilloscopes and LeCroy transient digital recorders.

Figure 2. Radiation intensity versus time record for shot 197 (a) on diopside glass, and for shot 141 (b) on diopside single-crystal, both at 750 nm. Duration of the sample radiation intensity is much shorter than that of the glass experiment shown in (a) because sample is thinner.

Figure 3. Spectral radiance data versus wavelength and greybody fits for $\hat{\epsilon}_{exp}(t_{exp})$ and $T_{exp}(t_{exp})$. The size of the data rectangles represent experimental uncertainty. Parts (a), (b) and (c) represent shot 140, 169 and 197 data, respectively.

Figure 4. Experimental results for crystal and glass Di, and model Hugoniots calculated with a range of values for the STP density of the HPP, ρ_i (a), the equilibrium thermodynamic Grüneisen parameter, γ_i (b), and the difference in specific internal energy between phases at STP, $\Delta e_i^{\alpha-\beta}$ (c).

Figure 5. Experimental and model pressure-temperature shock-compression results for HPP Di, along with experimentally constrained model results for B2-CaO (Boslough *et al.*, 1984), MgO (Svendsen and Ahrens, 1987), and SiO_2 stishovite and liquid (Lyzenga *et al.*, 1983). Also shown are the mantle temperature profiles of Stacey (1977) and Brown and Shankland (1980). The vertical line marks the pressure of the mantle-core boundary (135.7 GPa).

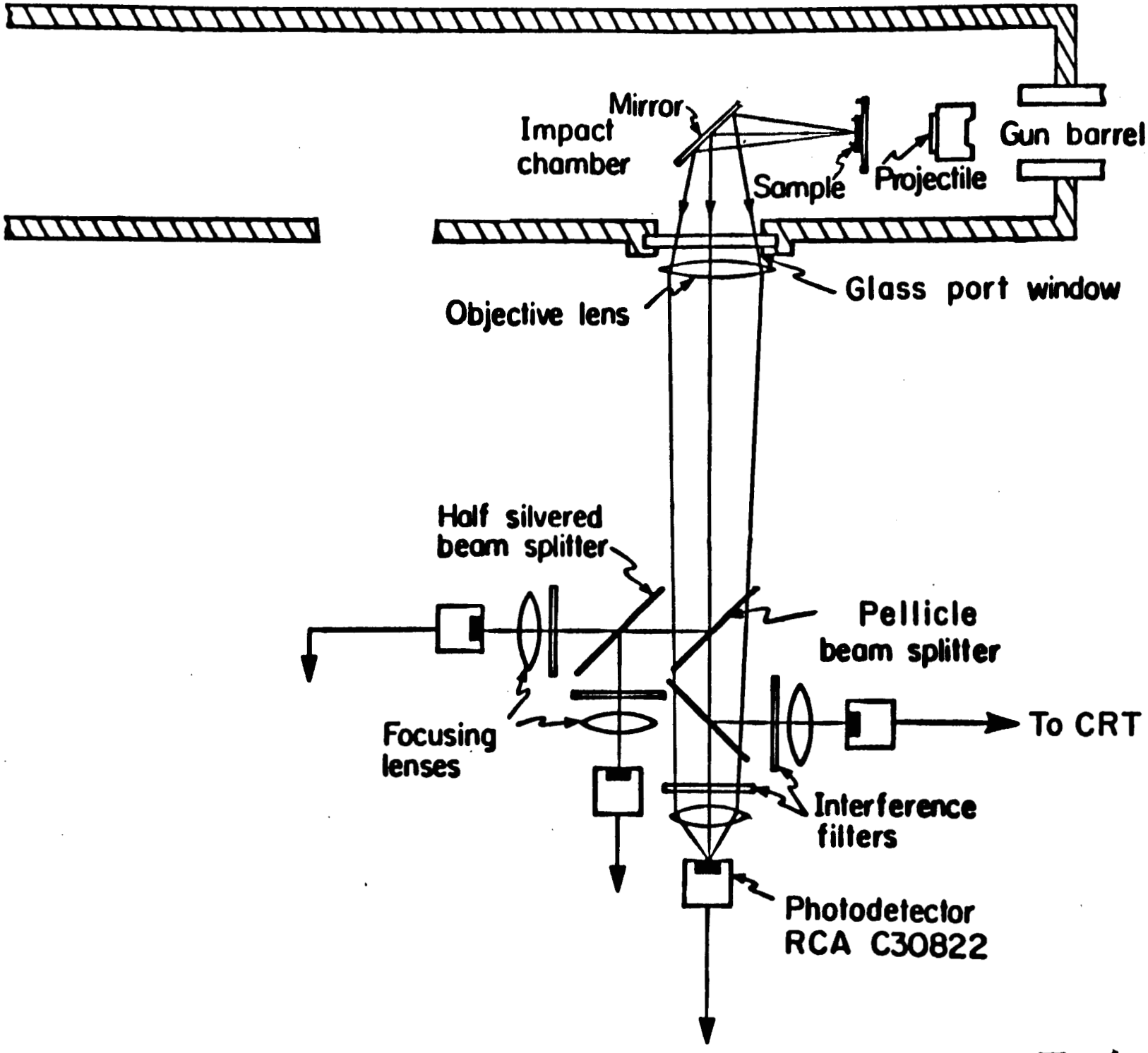
Mirror
Impact chamber
Sample
Projectile
Gun barrel
Glass port window
Objective lens
Half silvered beam splitter
Pellicle beam splitter
To CRT
Focusing lenses
Interference filters
Photodetector RCA C30822

Fig. 1

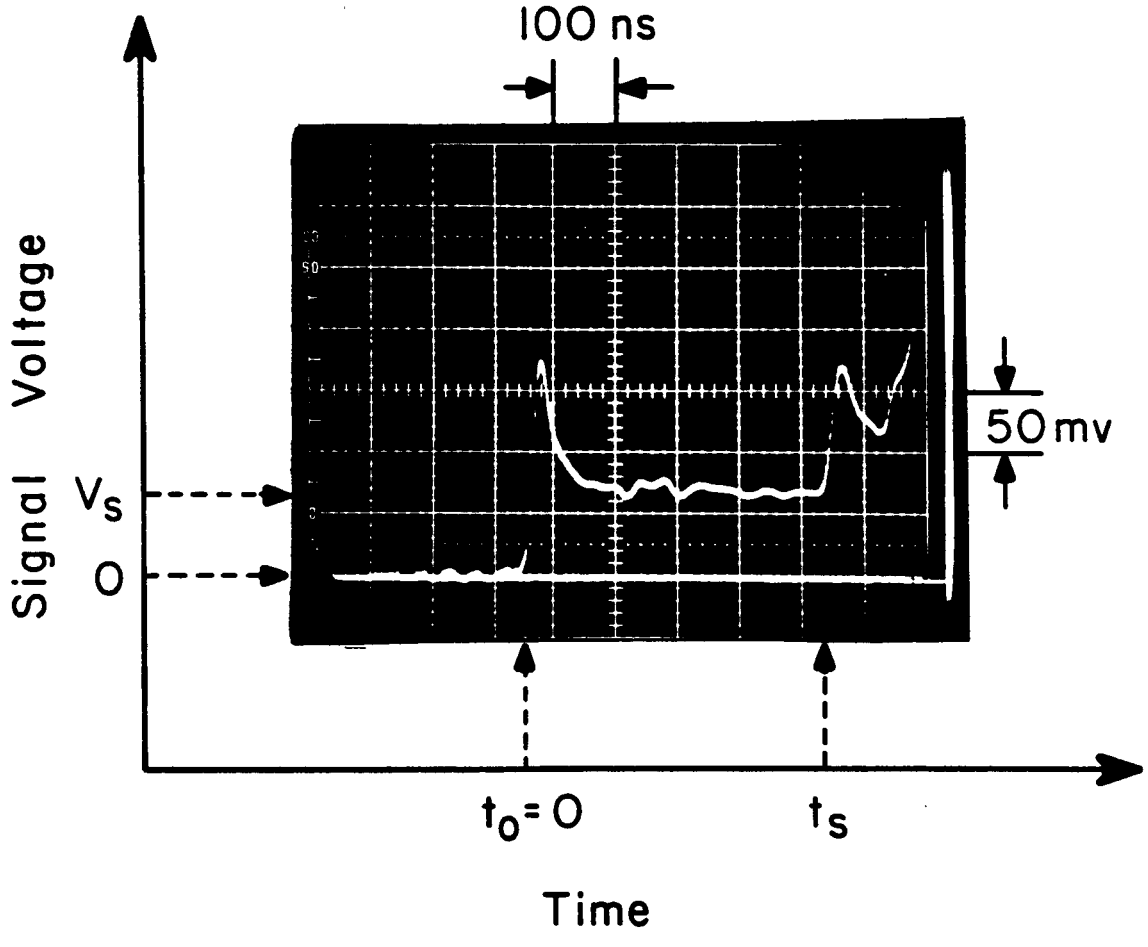

Fig 2a.

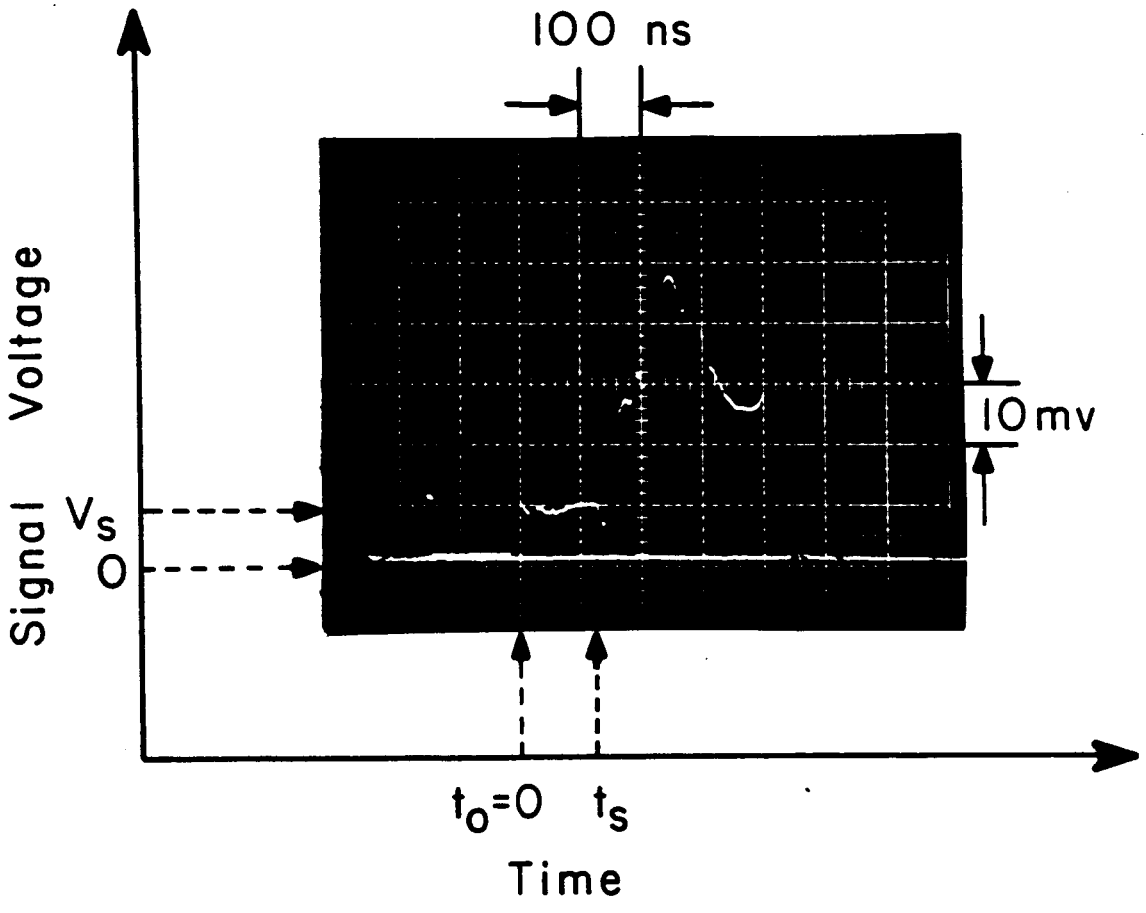

Fig. 2b.

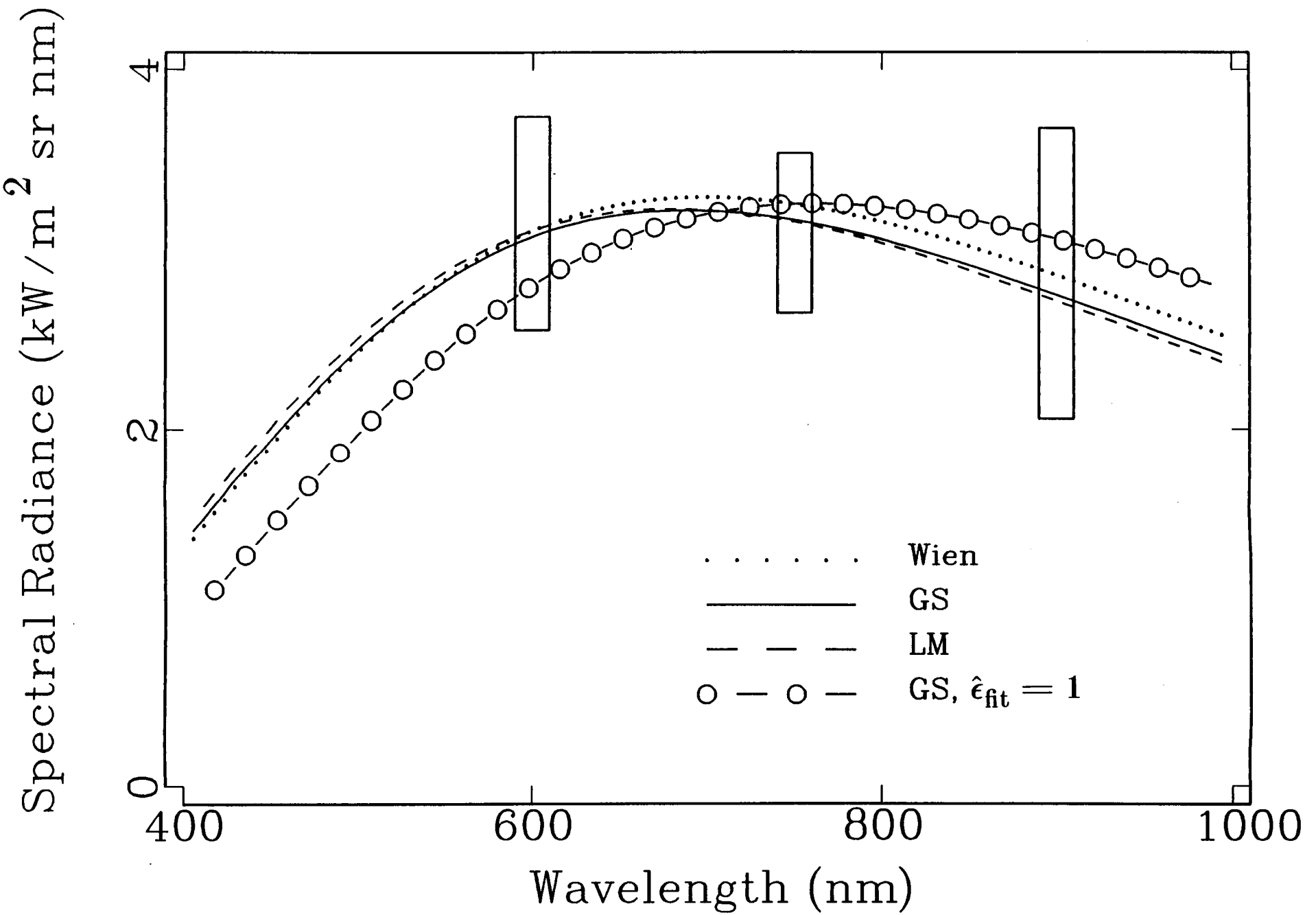
Spectral Radiance (kW/m^2 sr nm)
0
2
4
400
600
800
1000
Wavelength (nm)
Wien
GS
LM
GS, $\hat{\epsilon}_{\text{fit}} = 1$

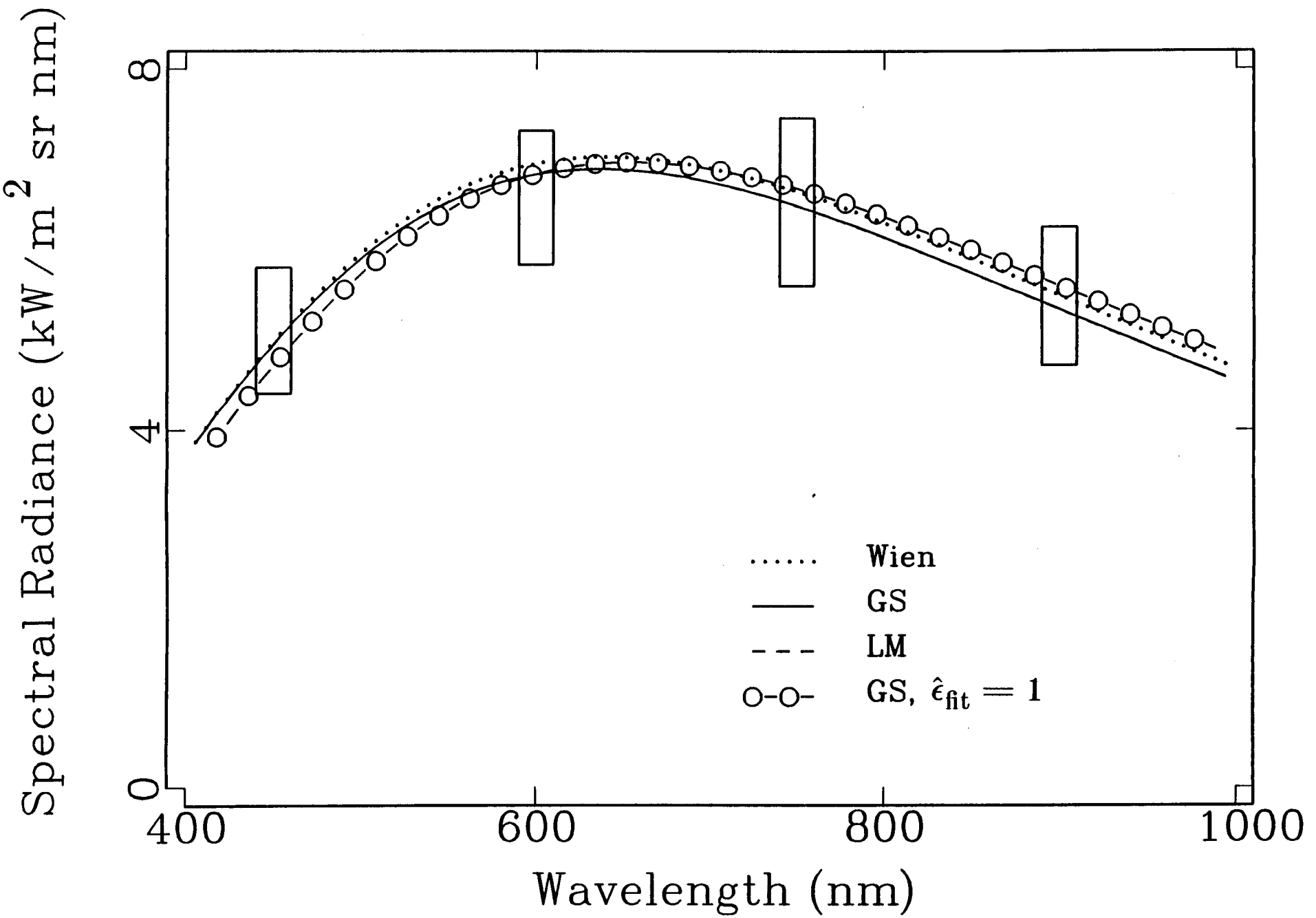
Spectral Radiance (kW/m^2 sr nm)
0
4
8
400
600
800
1000
Wavelength (nm)
Wien
GS
LM
GS, $\hat{\epsilon}_{fit} = 1$

3b

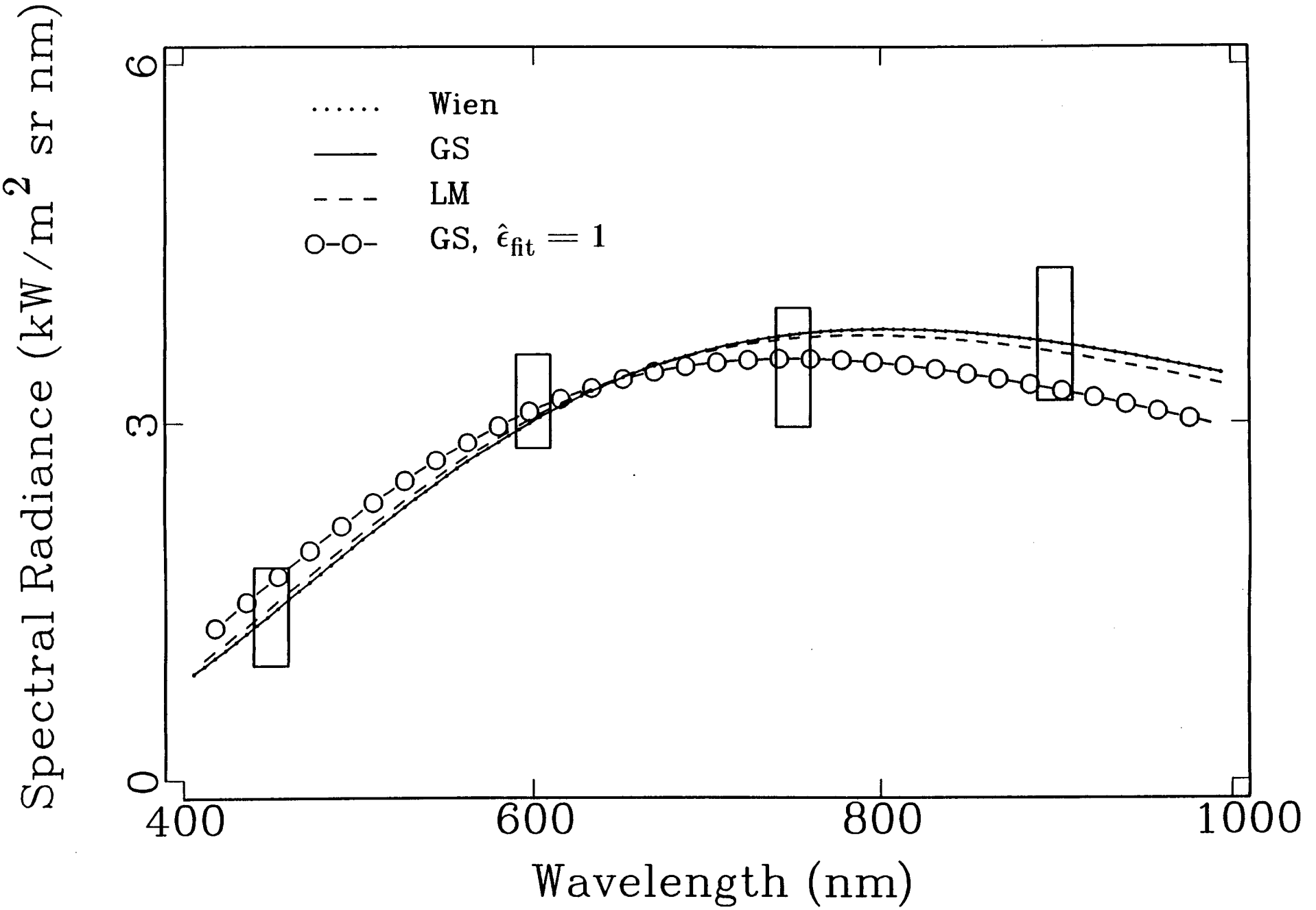
Spectral Radiance (kW/m^2 sr nm)
0
3
6
400
600
800
1000
Wavelength (nm)
Wien
GS
LM
GS, $\hat{\epsilon}_{fit} = 1$

3c.

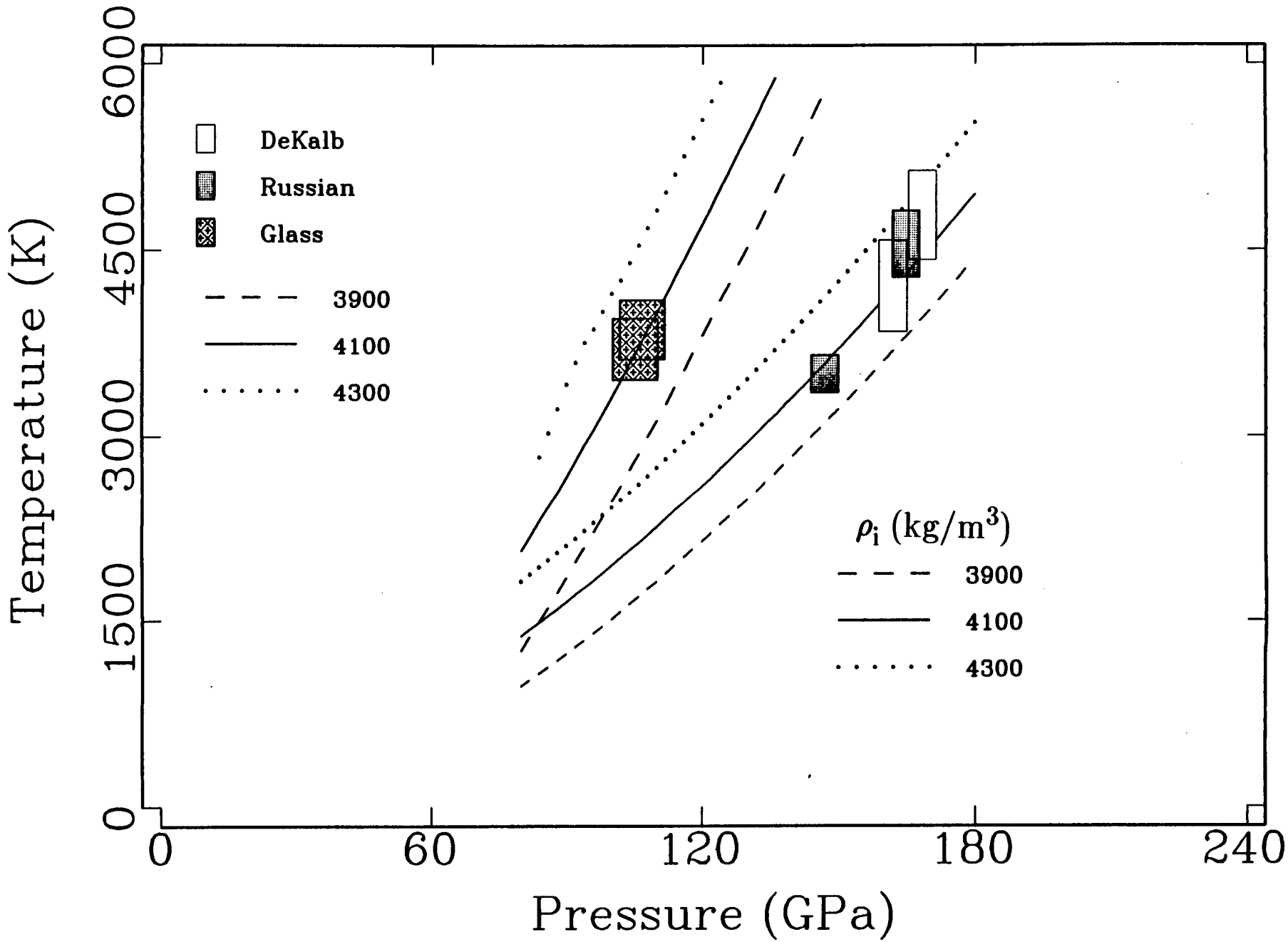
Temperature (K)
0
1500
3000
4500
6000
0
60
120
180
240
Pressure (GPa)
DeKalb
Russian
Glass
3900
4100
4300
ρ_i (kg/m^3)
3900
4100
4300

Fig 4a.

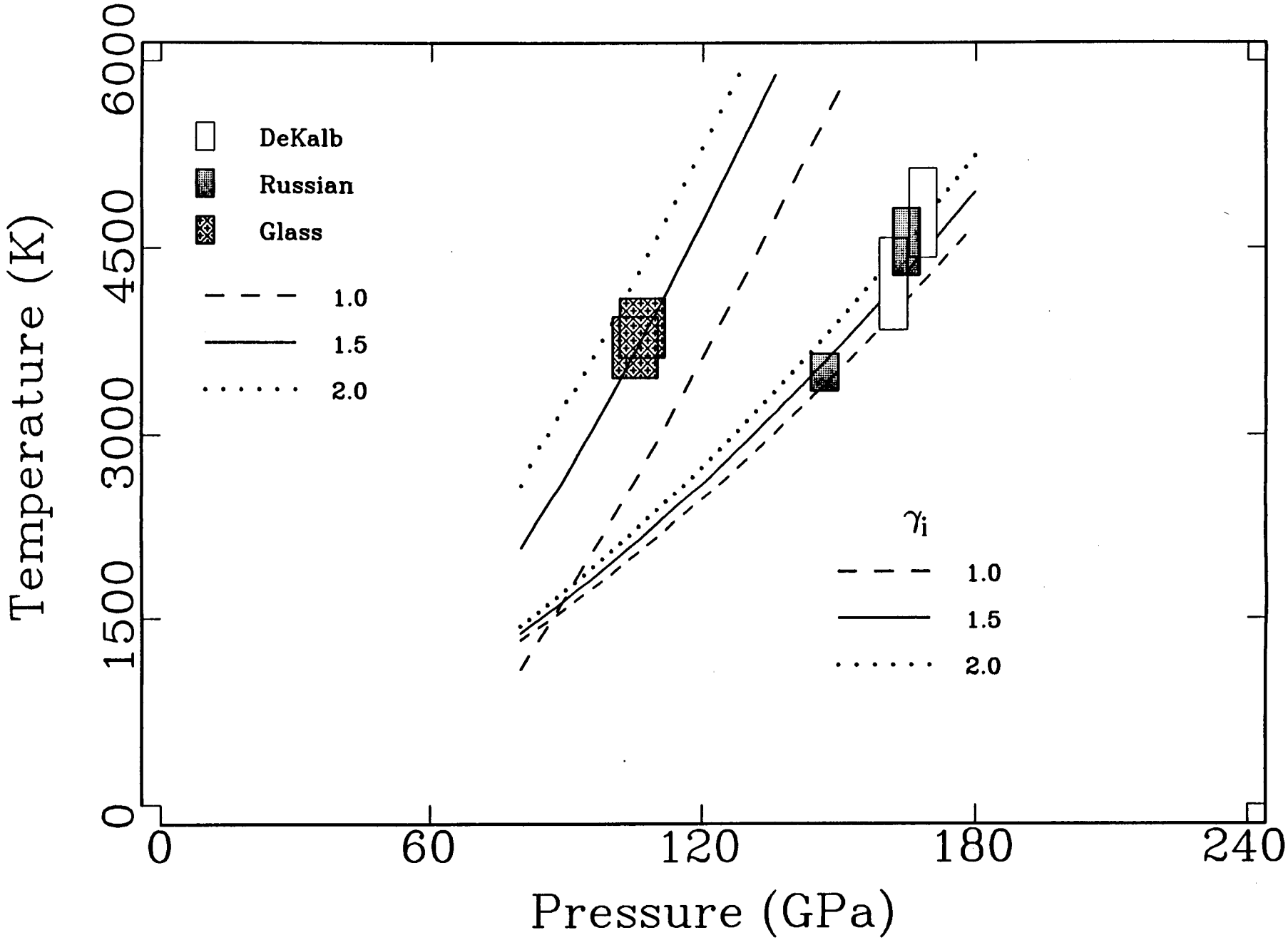
Temperature (K)
0
1500
3000
4500
6000
0
60
120
180
240
Pressure (GPa)
DeKalb
Russian
Glass
1.0
1.5
2.0
γ_i
1.0
1.5
2.0

4b.

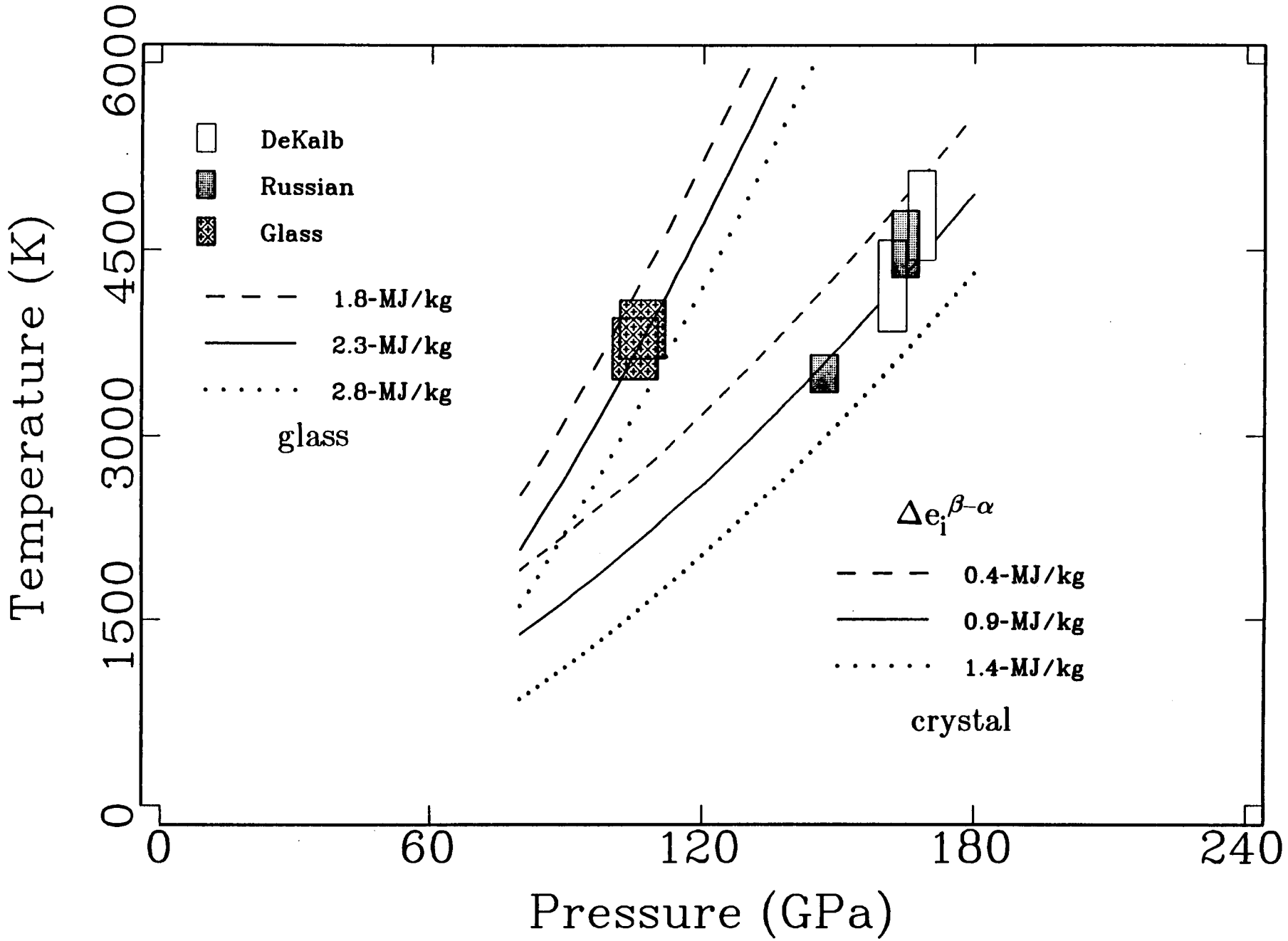
Temperature (K)
0
1500
3000
4500
6000
0
60
120
180
240
Pressure (GPa)
DeKalb
Russian
Glass
1.8-MJ/kg
2.3-MJ/kg
2.8-MJ/kg
glass
$\Delta e_i^{\beta-\alpha}$
0.4-MJ/kg
0.9-MJ/kg
1.4-MJ/kg
crystal

Fig 4c

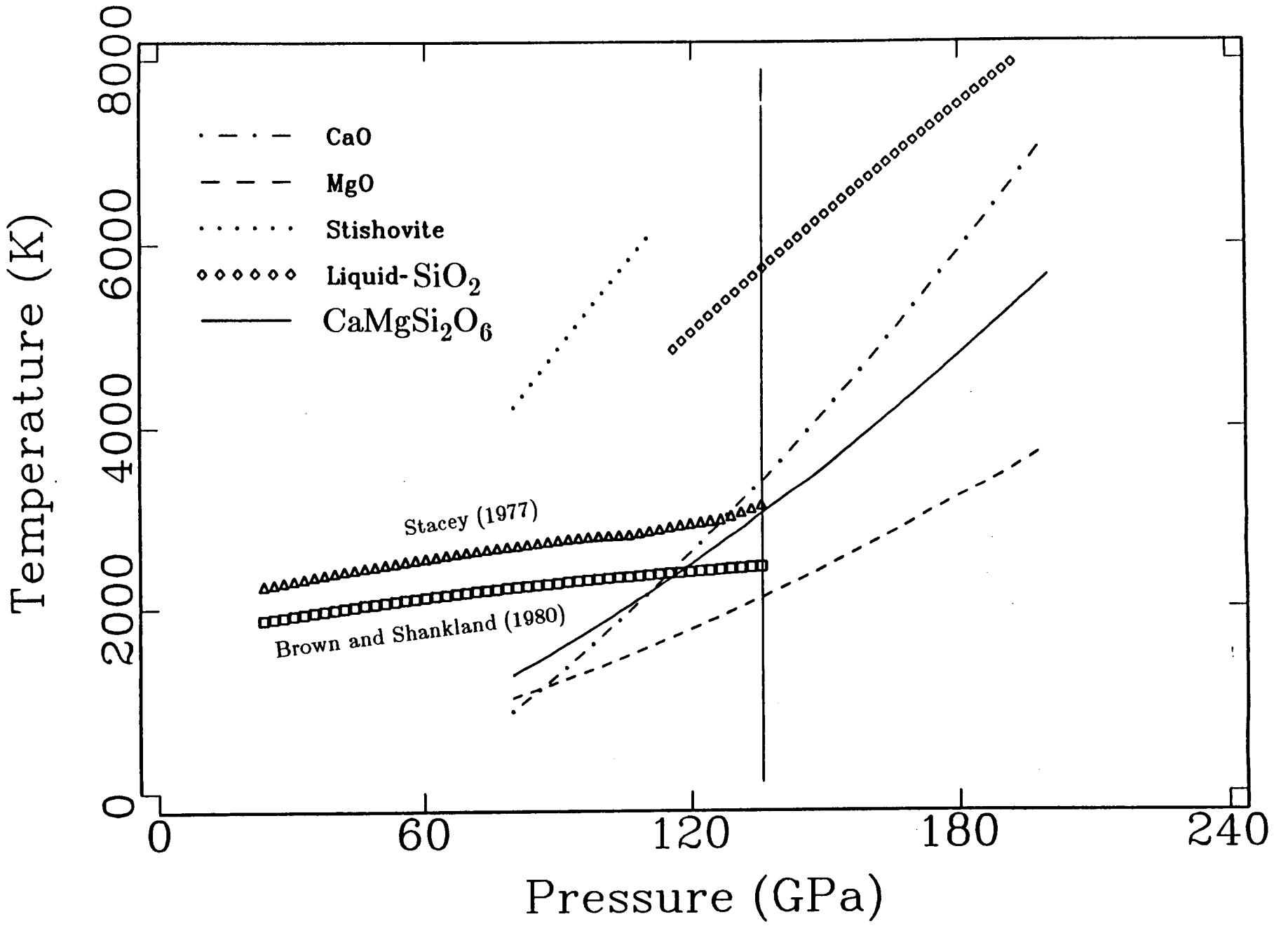
CaO
MgO
Stishovite
Liquid-SiO_2
$CaMgSi_2O_6$
Stacey (1977)
Brown and Shankland (1980)
Temperature (K)
0
2000
4000
6000
8000
0
60
120
180
240
Pressure (GPa)